J. Plasma Phys. (2020), *vol.* 86, 905860305
doi:10.1017/S0022377820000045

Particle trajectories in Weibel filaments: influence of external field obliquity and chaos

A. Bret[1,2,†] **and M. E. Dieckmann**[3]

[1]ETSI Industriales, Universidad de Castilla-La Mancha, 13071 Ciudad Real, Spain

[2]Instituto de Investigaciones Energéticas y Aplicaciones Industriales, Campus Universitario de Ciudad Real, 13071 Ciudad Real, Spain

[3]Department of Science and Technology (ITN), Linköping University, 60174 Norrköping, Sweden

(Received 7 October 2019; revised 15 January 2020; accepted 16 January 2020)

When two collisionless plasma shells collide, they interpenetrate and the overlapping region may turn Weibel unstable for some values of the collision parameters. This instability grows magnetic filaments which, at saturation, have to block the incoming flow if a Weibel shock is to form. In a recent paper (Bret, *J. Plasma Phys.*, vol. 82, 2016*b*, 905820403), it was found by implementing a toy model for the incoming particle trajectories in the filaments, that a strong enough external magnetic field $\boldsymbol{B}_0$ can prevent the filaments blocking the flow if it is aligned with them. Denoting by B_f the peak value of the field in the magnetic filaments, all test particles stream through them if $\alpha = B_0/B_f > 1/2$. Here, this result is extended to the case of an oblique external field B_0 making an angle θ with the flow. The result, numerically found, is simply $\alpha > \kappa(\theta)/\cos\theta$, where $\kappa(\theta)$ is of order unity. Noteworthily, test particles exhibit chaotic trajectories.

Key words: astrophysical plasmas, plasma flows, plasma nonlinear phenomena

1. Introduction

Collisionless plasmas can sustain shock waves with a front much smaller than the particle mean free path (Sagdeev & Kennel 1991). These shocks, which are mediated by collective plasma effects rather than binary collisions, have been dubbed 'collisionless shocks'. It is well known that the encounter of two collisional fluids generates two counter-propagating shock waves (Zel'dovich & Raizer 2002). Likewise, the encounter of two collisionless plasmas generate two counter-propagating collisionless shock waves (Forslund & Shonk 1970; Silva *et al.* 2003; Spitkovsky 2008; Ryutov 2018). In the collisional case, the shocks are launched when the two fluids make contact. In the collisionless case, the two plasmas start interpenetrating as the long mean free path prevents them from 'bumping' into each other. As a counter-streaming plasma system, the interpenetrating region quickly turns unstable. The instability grows, saturates and creates a localized turbulence which stops the incoming flow, initiating the density build-up in the overlapping region (Bret *et al.* 2013, 2014; Dieckmann & Bret 2017).

† Email address for correspondence: antoineclaude.bret@uclm.es

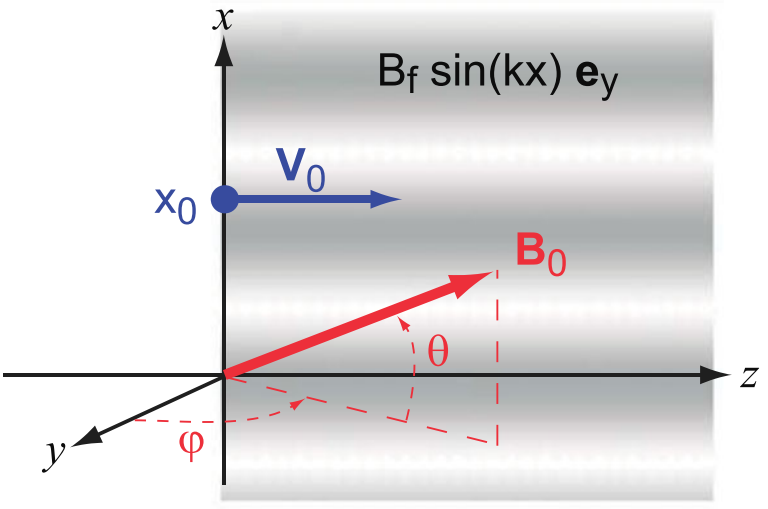

FIGURE 1. Set-up considered. We can consider $\varphi = \pi/2$ since the direction of the flow, the field and the $\boldsymbol{k}$ of the fastest growing Weibel mode, are coplanar for the fastest growing Weibel modes (Bret 2014; Novo, Bret & Sinha 2016).

Various kind of instabilities do grow in the overlapping region (Bret, Gremillet & Dieckmann 2010). However, the fastest growing one takes the lead and eventually defines the ensuing turbulence. When the system is such that the filamentation, or Weibel, instability grows faster, magnetic filaments are generated (Medvedev & Loeb 1999; Wiersma & Achterberg 2004; Lyubarsky & Eichler 2006; Kato 2007; Lemoine *et al.* 2019). In a pair plasma[1], the conditions required for the Weibel instability to lead the linear phase have been studied in Bret (2016*a*) for a flow-aligned field, and in Bret & Dieckmann (2017) for an oblique field. A mildly relativistic flow is required. Also, accounting for an oblique field supposes the Larmor radius of the particles is large compared to the dimensions of the system. Since the field modifies the hierarchy of unstable modes, it can prompt another mode than Weibel to lead the linear phase. In such cases, studies found so far that a shock still forms (Bret *et al.* 2017; Dieckmann & Bret 2017, 2018), mediated by the growth of the non-Weibel leading instability, like a two-stream for example.

Since the blocking of the flow entering the filaments is key for the shock formation, it is interesting to study under which conditions a test particle will be stopped in these magnetic filaments. Recently, a toy model of the process successfully reproduced the criteria for shock formation in the case of pair plasmas (Bret 2015). When implemented accounting for a flow-aligned magnetic field (Bret 2016*b*), the same kind of model could predict how too strong a field can deeply affect the shock formed (Bret *et al.* 2017; Bret & Narayan 2018). In view of the many settings involving oblique magnetic fields, we extend here the previous model to the case of an oblique field.

The system considered is sketched in figure 1. The half-space $z \geqslant 0$ is filled with the magnetic filaments $\boldsymbol{B}_f = B_f \sin(kx)\ \boldsymbol{e}_y$. In principle, we should consider any possible

[1]To our knowledge, there is no systematic study of the hierarchy of unstable modes for two magnetized colliding ion/electron plasma shells. See Lyubarsky & Eichler (2006), Yalinewich & Gedalin (2010) and Shaisultanov, Lyubarsky & Eichler (2012) for works contemplating the un-magnetized case.

https://doi.org/10.1017/S0022377820000045 Published online by Cambridge University Press

orientation for $\boldsymbol{B}_0$, thus having to consider the angles θ and φ. Yet, previous works in a three-dimensional geometry found that the fastest growing Weibel modes are found with a wave vector coplanar with the field $\boldsymbol{B}_0$ and the direction of the flow (Bret 2014; Novo *et al.* 2016). Here, the initial flow giving rise to Weibel is along z and we set up the axis so that $\boldsymbol{k}$ is along x. We can therefore consider $\varphi = \pi/2$ so that $\boldsymbol{B}_0 = B_0(\sin\theta, 0, \cos\theta)$.

A test particle is injected at $(x_0, 0, 0)$ with velocity $\boldsymbol{v}_0 = (0, 0, v_0)$ and Lorentz factor $\gamma_0 = (1 - v_0^2/c^2)^{-1/2}$, mimicking a particle of the flow entering the filamented overlapping region. Our goal is to determine under which conditions the particle streams through the magnetic filaments to $z = +\infty$, or is trapped inside. As explained in previous articles (Bret 2015, 2016*b*), in the present toy model, this dichotomy comes down to determining whether test particles stream through the filaments, or bounce back to the region $z < 0$. The reason for this is that, in a more realistic setting, particles reaching the filaments and turning back will likely be trapped in the turbulent region between the upstream and the downstream. This problem is clearly related to that of the shock formation, since the density build-up leading to the shock requires the incoming flow to be trapped in the filaments.

2. Equations of motion

Since the Lorentz factor γ_0 is a constant of the motion, the equation of motion for our test particle of mass m and charge q reads,

$$m\gamma_0\ddot{\boldsymbol{x}} = q\frac{\dot{\boldsymbol{x}}}{c} \times (\boldsymbol{B}_f + \boldsymbol{B}_0). \tag{2.1}$$

Explaining each component, we find for $z > 0$,

$$\ddot{x} = \frac{qB_f}{\gamma_0 mc}\left[\frac{B_0}{B_f}\dot{y}\cos\theta - \dot{z}\sin kx\right], \tag{2.2}$$

$$\ddot{y} = \frac{qB_f}{\gamma_0 mc}\frac{B_0}{B_f}[\dot{z}\sin\theta - \dot{x}\cos\theta], \tag{2.3}$$

$$\ddot{z} = \frac{qB_f}{\gamma_0 mc}\left[-\frac{B_0}{B_f}\dot{y}\sin\theta + \dot{x}\sin kx\right], \tag{2.4}$$

while $B_f = 0$ for $z < 0$. We can now define the following dimensionless variables,

$$\boldsymbol{X} = k\boldsymbol{x}, \quad \alpha = \frac{B_0}{B_f}, \quad \tau = t\omega_{B_f}, \quad \text{with } \omega_{B_f} = \frac{qB_f}{\gamma_0 mc}. \tag{2.5a–d}$$

With these variables, the system (2.2)–(2.4) reads,

$$\left.\begin{aligned} \ddot{X} &= -\dot{Z}\mathcal{H}(Z)\sin X + \alpha\dot{Y}\cos\theta, \\ \ddot{Y} &= \alpha(\dot{Z}\sin\theta - \dot{X}\cos\theta), \\ \ddot{Z} &= \dot{X}\mathcal{H}(Z)\sin X - \alpha\dot{Y}\sin\theta, \end{aligned}\right\} \tag{2.6}$$

where $\mathcal{H}$ is the Heaviside step function $\mathcal{H}(x) = 0$ for $x < 0$ and $\mathcal{H}(x) = 1$ for $x \geqslant 0$. The initial conditions are,

$$\left.\begin{aligned} \boldsymbol{X}(\tau = 0) &= (X_0, 0, 0) \quad \text{with } X_0 \equiv kx_0, \\ \dot{\boldsymbol{X}}(\tau = 0) &= (0, 0, \dot{Z}_0) \quad \text{with } \dot{Z}_0 \equiv \frac{kv_0}{\omega_{B_f}}. \end{aligned}\right\} \tag{2.7}$$

https://doi.org/10.1017/S0022377820000045 Published online by Cambridge University Press

3. Constants of the motion and chaotic behaviour

The total field in the region $z > 0$ reads $\boldsymbol{B} = (B_0 \sin\theta, B_f \sin(kx), B_0 \cos\theta)$. It can be written as $\boldsymbol{B} = \nabla \times \boldsymbol{A}$, with the vector potential in the Coulomb gauge,

$$\boldsymbol{A} = \begin{pmatrix} 0 \\ B_0 x \cos\theta \\ B_0 y \sin\theta + B_f \dfrac{\cos(kx)}{k} \end{pmatrix}. \tag{3.1}$$

The canonical momentum then reads (Jackson 1998),

$$\boldsymbol{P} = \boldsymbol{p} + \frac{q}{c}\boldsymbol{A} = \begin{pmatrix} p_x \\ p_y + \dfrac{q}{c} B_0 x \cos\theta \\ p_z + \dfrac{q}{c}\left(B_0 y \sin\theta + B_f \dfrac{\cos(kx)}{k} \right) \end{pmatrix}, \tag{3.2}$$

where $\boldsymbol{p} = \gamma_0 m \boldsymbol{v}$. Since it does not explicitly depend on z, the z component is a constant of the motion. It can equally be obtained by time integrating (2.4). Note that for $\theta = 0$, the y dependence vanishes so that the y component of the canonical momentum is also a constant of the motion (Bret 2016*b*).

We can derive another constant of the motion from (2.3). Time integrating it and remembering $\dot{y}(t=0) = z(t=0) = 0$, we find,

$$\dot{y} = \frac{qB_0}{\gamma_0 mc}[z \sin\theta - (x - x_0)\cos\theta]. \tag{3.3}$$

Since x_0 is obviously a constant, we can express it in terms of the other variables and obtain an invariant, that is

$$\begin{aligned} x_0 &= x - z\tan\theta + \frac{c}{qB_0 \cos\theta}\gamma_0 m\dot{y} \\ &= x - z\tan\theta + \frac{c}{qB_0\cos\theta}\left(P_y - \frac{q}{c}A_y\right). \end{aligned} \tag{3.4}$$

Finally, the Hamiltonian,

$$\mathcal{H} = c\sqrt{c^2 m^2 + \left(\boldsymbol{P} - \frac{q}{c}\boldsymbol{A}\right)^2}, \tag{3.5}$$

is also a constant of the motion. Replacing A_y in (3.4) by its expression from (3.1), we therefore have the following constants of the motion,

$$\mathcal{H} \equiv C_1 = c\sqrt{c^2 m^2 + \left(\boldsymbol{P} - \frac{q}{c}\boldsymbol{A}\right)^2}, \tag{3.6}$$

$$C_2 = P_z, \tag{3.7}$$

$$x_0 \equiv C_3 = \frac{c}{qB_0\cos\theta}P_y - z\tan\theta. \tag{3.8}$$

According to Liouville's theorem on integrable systems, an n-dimensional Hamiltonian system is integrable if it has n constants of motion $C_j(x_i, P_i, t)_{j\in[1\ldots n]}$

https://doi.org/10.1017/S0022377820000045 Published online by Cambridge University Press

in involution (Chen & Palmadesso 1986; Ott 2002; Lichtenberg & Lieberman 2013), that is,

$$\{C_j, C_k\} = \sum_{i=1}^{3} \left(\frac{\partial C_j}{\partial x_i} \frac{\partial C_k}{\partial P_i} - \frac{\partial C_k}{\partial x_i} \frac{\partial C_j}{\partial P_i} \right) = 0, \quad \forall (j, k), \tag{3.9}$$

where $\{f, g\}$ is the Poisson bracket of f and g. It is easily checked that, $C_{2,3}$ being constants of the motion, $\{\mathcal{H}, C_2\} = \{\mathcal{H}, C_3\} = 0$. However,

$$\{C_2, C_3\} = -\tan\theta. \tag{3.10}$$

As a result, the system is integrable only for $\theta = 0$ (Bret 2016*b*). Otherwise, it is chaotic, as will be checked numerically in the following sections.

4. Reduction of the number of free parameters

The free parameters of the system (2.2)–(2.4) with initial conditions (2.7) are $(X_0, \dot{Z}_0, \alpha, \theta)$. In order to deal with a more tractable phase space parameter, we now reduce its dimension, accounting for the physical context of the problem.

Consider the magnetic filaments generated by the growth of the filamentation instability triggered by the counter-streaming of 2 cold (thermal spread $\Delta v \ll v$) symmetric pair plasmas. Both plasma shells have identical density n in the laboratory frame, and initial velocities $\pm v\boldsymbol{e}_z$. We denote $\beta = v/c$. The Lorentz factor γ_0 previously defined equally reads $\gamma_0 = (1-\beta^2)^{-1/2}$ since the test particles entering the magnetic filaments belong to the same plasma shells.

The wave vector $\boldsymbol{k}$ defining the magnetic filaments is also the wave vector of the fastest growing filamentation modes. We can then set (Bret *et al.* 2013),

$$k = \frac{\omega_p}{c\sqrt{\gamma_0}}, \tag{4.1}$$

where $\omega_p^2 = 4\pi n q^2/m$, so that,

$$\dot{Z}_0 = \frac{\beta}{\sqrt{\gamma_0}} \frac{\omega_p}{\omega_{B_f}} = \frac{\beta}{\sqrt{\gamma_0}} \frac{\omega_{B_0}}{\omega_{B_f}} \frac{\omega_p}{\omega_{B_0}} = \frac{\beta}{\sqrt{\gamma_0}} \alpha \frac{\omega_p}{\omega_{B_0}}, \tag{4.2}$$

where,

$$\omega_{B_0} = \frac{qB_0}{\gamma_0 mc}. \tag{4.3}$$

The peak field B_f in the filaments can be estimated from the growth rate δ of the instability, considering $\omega_{B_f} \sim \delta$ (Davidson *et al.* 1972; Grassi *et al.* 2017). It turns out that, over the domain $\delta \gg \omega_{B_0}$, the growth rate δ depends weakly on θ and can be well approximated by (Stockem, Lerche & Schlickeiser 2006; Bret 2014),

$$\omega_{B_f} \sim \delta = \omega_p \sqrt{\frac{2\beta^2}{\gamma_0} - \left(\frac{\omega_{B_0}}{\omega_p}\right)^2}, \tag{4.4}$$

so that,

$$\omega_{B_f} = \frac{\omega_{B_0}}{\alpha} = \omega_p \sqrt{\frac{2\beta^2}{\gamma_0} - \left(\frac{\omega_{B_0}}{\omega_p}\right)^2}. \tag{4.5}$$

https://doi.org/10.1017/S0022377820000045 Published online by Cambridge University Press

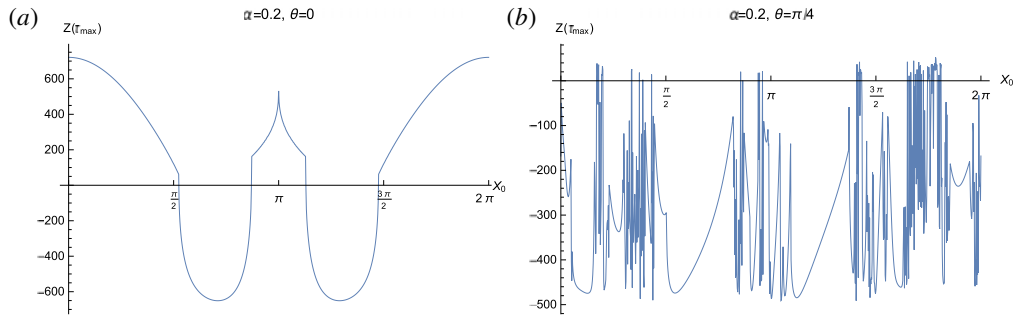

FIGURE 2. Value of $Z(\tau_{\max})$ in terms of X_0 for $\tau_{\max} = 10^3$ and two values of θ.

This expression allows us to express ω_{B_0}/ω_p as,

$$\frac{\omega_{B_0}}{\omega_p} = \sqrt{\frac{2}{\gamma_0}}\frac{\alpha\beta}{\sqrt{1+\alpha^2}}, \tag{4.6}$$

so that (4.2) eventually reads,

$$\dot{Z}_0 = \sqrt{\frac{1+\alpha^2}{2}}. \tag{4.7}$$

The parameters phase space is thus reduced to three dimensions, (X_0, α, θ).

5. Numerical exploration

It was previously found that, for $\theta = 0$, all particles stream through the filaments, no matter their initial position and velocity, if $\alpha > 1/2$ (Bret 2016*b*). Clearly, for $\theta = \pi/2$, no particle can stream to $z = +\infty$. As we shall see, the θ-dependent threshold value of α beyond which all particles go to ∞ is simply $\propto 1/\cos\theta$.

The system (2.6)–(2.7) is solved using the *Mathematica* 'NDSolve' function. The equations are invariant under the change $X \to X + 2\pi$, so that we can restrict the investigation to $X_0 \in [-\pi, \pi]$. Unless $\theta = 0$, there are no other trivial symmetries. In particular, the transformation $\theta \to -\theta$ does not leave the system invariant. We shall detail the case $\theta \in [0, \pi/2]$ and only give the results, which are very similar although not identical, for $\theta \in [-\pi/2, 0]$.

The numerical exploration is conducted by solving the equations and looking for the value of Z at a large time $\tau = \tau_{\max}$. Figure 2 shows the value of $Z(\tau_{\max})$ in terms of $X_0 \in [0, 2\pi]$ for the specified values of (α, θ) and $\tau_{\max} = 10^3$. Similar results have been obtained for larger values of τ like $\tau = 10^4$, or even smaller ones, such as $\tau = 500$. For $\theta = \pi/4$, save a few exceptions for some values of X_0, all particles bounced back to the $z < 0$ region. As explained in Bret (2015, 2016*b*), this means that, in a more realistic setting, they would likely be trapped in the filaments.

As evidenced by figure 2(*a*), the function $Z(\tau_{\max})$ is smooth for $\theta = 0$. Yet, for $\theta = \pi/4$ (*b*), the result features regions where $Z(\tau_{\max})$ varies strongly with X_0. In order to identify chaos, figure 3 presents a series of successive zooms of figure 2(*b*), where the function $Z(\tau_{\max})$ is plotted over an increasingly small X_0 interval inside $X_0 \in [\pi/4, \pi/2]$.

https://doi.org/10.1017/S0022377820000045 Published online by Cambridge University Press

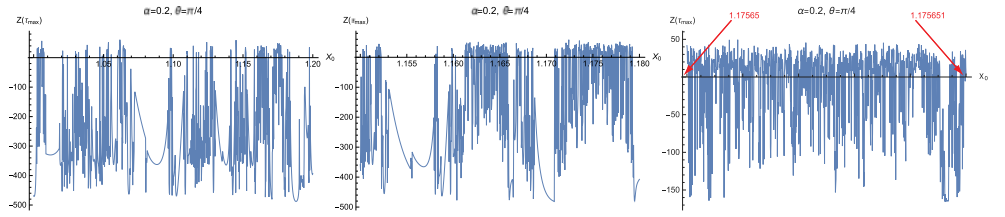

FIGURE 3. Value of $Z(\tau_{\max})$ for $\theta = \pi/4$ and increasingly small X_0 intervals.

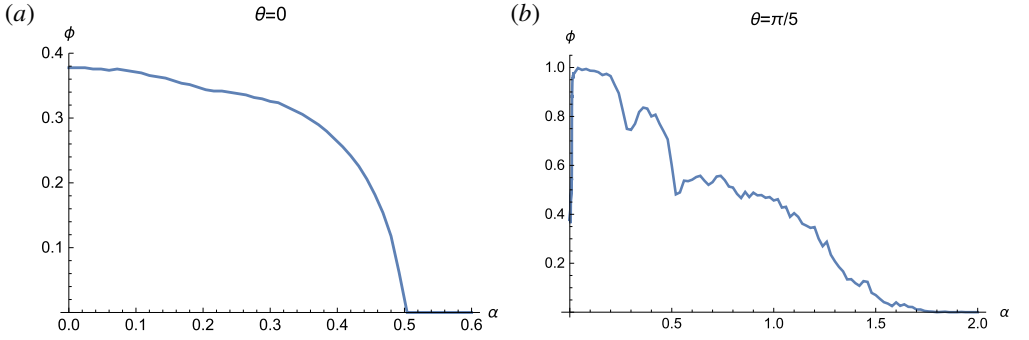

FIGURE 4. Plot on the function ϕ defined by (5.1), in terms of α and for $\theta = 0$ and $\pi/5$.

As expected from the analysis conducted in § 3, the system is chaotic. Note that chaotic trajectories in magnetic field lines have already been identified in the literature (Chen & Palmadesso 1986; Büchner & Zelenyi 1989; Ram & Dasgupta 2010; Cambon *et al.* 2014).

Figure 2 has been plotted by solving the system for $N + 1$ particles shot from $X_0(j) = j2\pi/N$ with $j = 0 \ldots N$. We denote by $Z_j(\tau_{\max})$ the value of Z reached by the jth particle at $\tau = \tau_{\max}$. Then, we define the following function,

$$\phi(\alpha, \theta) = \frac{1}{N+1} \sum_{j=0}^{N} \mathcal{H}[-Z_j(\tau_{\max})], \tag{5.1}$$

where $\mathcal{H}$ is again the Heaviside function.

The function ϕ represents therefore the fraction of particles that bounced back against the magnetic filaments. Figure 4(*a*) plots it in terms of α for $\theta = 0$. For $\alpha = 0$, that is $B_0 = 0$, approximately 40 % of the particles bounce back, i.e. are trapped in the filaments. As α is increased, the field $\boldsymbol{B}_0$ guides the test particles more and more efficiently until $\alpha \sim 0.5$, where all the particles stream through the filaments. In turn, figure 4(*b*) displays the case $\theta = \pi/5$. Being oblique, the field $\boldsymbol{B}_0$ is less efficient in guiding the particles through the filaments, and more efficient in trapping them inside. As a result, it takes a higher value of B_0, that is, $\alpha = 1.4$, to reach $\phi = 0$.

Similar numerical calculations have been conducted for various values of $\theta \in [0, \pi/2]$. We finally define $\alpha_c(\theta)$ as,

$$\phi(\alpha_c) = 0. \tag{5.2}$$

Here, $\alpha_c(\theta)$ is therefore the threshold value of α beyond which all particles bounce back against the filamented region, i.e. $\phi(\alpha \geqslant \alpha_c) = 0$. It is plotted in figure 5 and can

https://doi.org/10.1017/S0022377820000045 Published online by Cambridge University Press

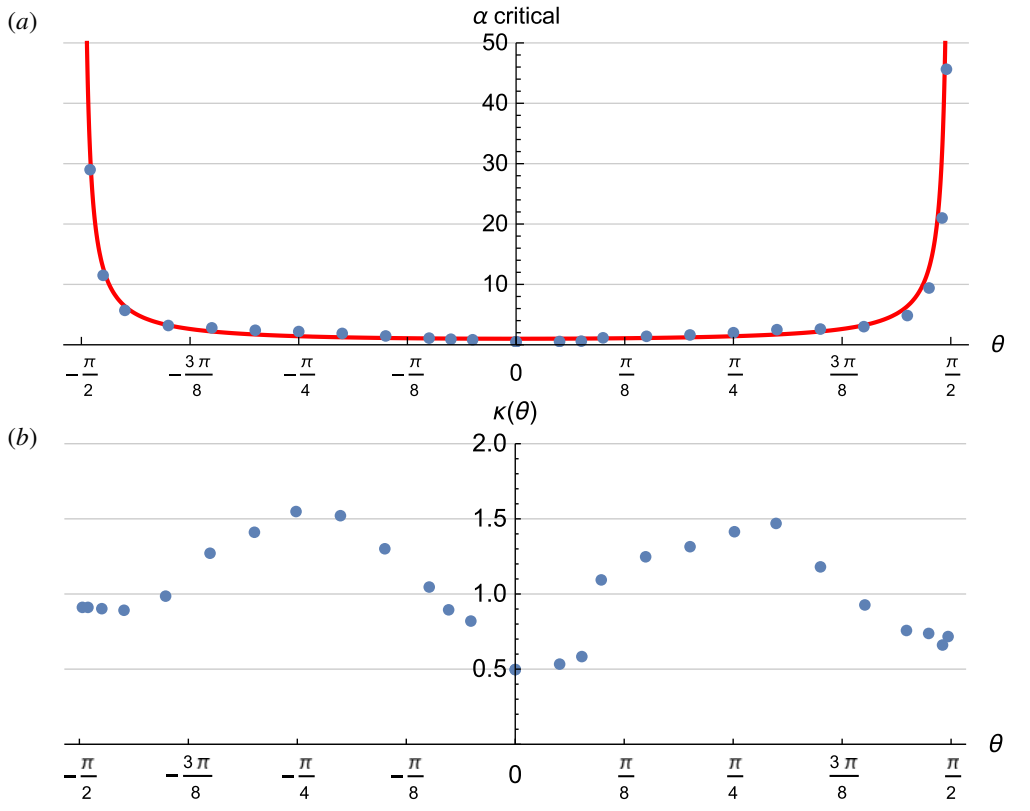

FIGURE 5. (*a*) Numerical computation of $\alpha_c(\theta)$ (blue dots) compared to $1/\cos\theta$ (red line). (*b*) Values of the $\kappa(\theta)$ function entering the expression of α_c in (5.3), in terms of θ.

be well approximated by,

$$\alpha_c = \kappa(\theta)\frac{1}{\cos\theta}, \tag{5.3}$$

where $\kappa(\theta)$ is of order unity (see figure 5*b*).

5.1. *Case* $\theta < 0$

As already noticed, there is no invariance by the change $\theta \to -\theta$. Figure 6 plots the counterpart of figure 2(*b*), but for $\theta = -\pi/4$. Although quite similar, the results are not identical. The numerical analysis detailed above for $\theta \in [0, \pi/2]$ has been conducted for $\theta \in [-\pi/2, 0]$. The function $\alpha_c(\theta < 0)$ again adjusts very well to the right-hand side of (5.3), with the values of $\kappa(\theta)$ plotted in figure 5(*b*).

6. Conclusion

A model previously developed to study test particle trapping in magnetic filaments has been extended to the case of an oblique external magnetic field. The result makes perfect physical sense: up to a constant κ of order unity, only the component of the field parallel to the filaments is relevant. The criterion obtained in Bret (2016*b*) for a

https://doi.org/10.1017/S0022377820000045 Published online by Cambridge University Press

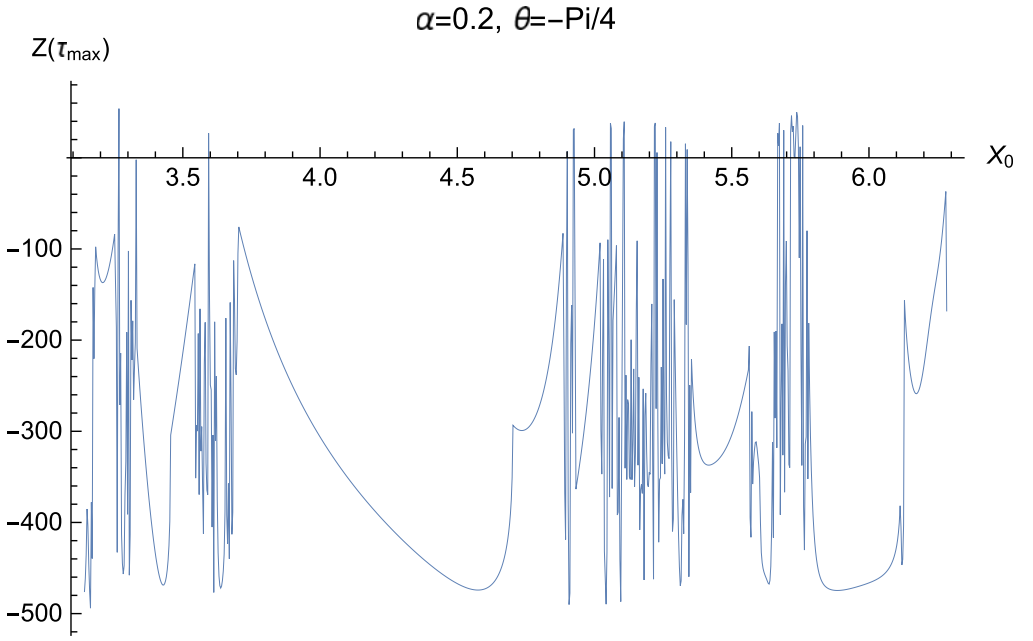

FIGURE 6. Same as figure 2(*b*), but for $\theta = -\pi/4$.

flow-aligned field, namely that particles are trapped if $\alpha > 1/2$, now reads,

$$\alpha > \frac{\kappa(\theta)}{\cos\theta}, \tag{6.1}$$

where $\kappa(\theta)$ is of order unity. As a consequence, a parallel field affects the shock more than an oblique one. Kinetic effects triggered by a parallel field can significantly modify the shock structure while a perpendicular field will rather 'help' the shock formation. This is in agreement with theoretical works which found a parallel field can divide by 2 the density jump expected from the Magnetohydrodynamic (MHD) Rankine–Hugoniot conditions (Bret *et al.* 2017; Bret & Narayan 2018), while the departure from MHD is less pronounced in the perpendicular case (Bret & Narayan 2019).

Acknowledgements

A.B. acknowledges support by grants ENE2016-75703-R from the Spanish Ministerio de Educación and SBPLY/17/180501/000264 from the Junta de Comunidades de Castilla-La Mancha. Thanks are due to I. Kourakis and D. Bénisti for enriching discussions.

REFERENCES

BRET, A. 2014 Robustness of the filamentation instability in arbitrarily oriented magnetic field: full three dimensional calculation. *Phys. Plasmas* **21** (2), 022106.

BRET, A. 2015 Particles trajectories in magnetic filaments. *Phys. Plasmas* **22**, 072116.

https://doi.org/10.1017/S0022377820000045 Published online by Cambridge University Press

BRET, A. 2016*a* Hierarchy of instabilities for two counter-streaming magnetized pair beams. *Phys. Plasmas* **23**, 062122.

BRET, A. 2016*b* Particles trajectories in Weibel magnetic filaments with a flow-aligned magnetic field. *J. Plasma Phys.* **82**, 905820403.

BRET, A. & DIECKMANN, M. E. 2017 Hierarchy of instabilities for two counter-streaming magnetized pair beams: influence of field obliquity. *Phys. Plasmas* **24** (6), 062105.

BRET, A., GREMILLET, L. & DIECKMANN, M. E. 2010 Multidimensional electron beam-plasma instabilities in the relativistic regime. *Phys. Plasmas* **17**, 120501.

BRET, A. & NARAYAN, R. 2018 Density jump as a function of magnetic field strength for parallel collisionless shocks in pair plasmas. *J. Plasma Phys.* **84**, 905840604.

BRET, A. & NARAYAN, R. 2019 Density jump as a function of magnetic field for collisionless shocks in pair plasmas: the perpendicular case. *Phys. Plasmas* **26**, 062108.

BRET, A., PE'ER, A., SIRONI, L., SĄDOWSKI, A. & NARAYAN, R. 2017 Kinetic inhibition of magnetohydrodynamics shocks in the vicinity of a parallel magnetic field. *J. Plasma Phys.* **83**, 715830201.

BRET, A., STOCKEM, A., FIUZA, F., RUYER, C., GREMILLET, L., NARAYAN, R. & SILVA, L. O. 2013 Collisionless shock formation, spontaneous electromagnetic fluctuations, and streaming instabilities. *Phys. Plasmas* **20** (4), 042102.

BRET, A., STOCKEM, A., NARAYAN, R. & SILVA, L. O. 2014 Collisionless Weibel shocks: full formation mechanism and timing. *Phys. Plasmas* **21** (7), 072301.

BÜCHNER, J. & ZELENYI, L. M. 1989 Regular and chaotic charged particle motion in magnetotaillike field reversals: 1. Basic theory of trapped motion. *J. Geophys. Res.* **94** (A9), 11821–11842.

CAMBON, B., LEONCINI, X., VITTOT, M., DUMONT, R. & GARBET, X. 2014 Chaotic motion of charged particles in toroidal magnetic configurations. *Chaos* **24** (3), 033101.

CHEN, J. & PALMADESSO, P. J. 1986 Chaos and nonlinear dynamics of single-particle orbits in a magnetotaillike magnetic field. *J. Geophys. Res.* **91**, 1499–1508.

DAVIDSON, R. C., HAMMER, D. A., HABER, I. & WAGNER, C. E. 1972 Nonlinear development of electromagnetic instabilities in anisotropic plasmas. *Phys. Fluids* **15**, 317.

DIECKMANN, M. E. & BRET, A. 2017 Simulation study of the formation of a non-relativistic pair shock. *J. Plasma Phys.* **83** (1), 905830104.

DIECKMANN, M. E. & BRET, A. 2018 Electrostatic and magnetic instabilities in the transition layer of a collisionless weakly relativistic pair shock. *Mon. Not. R. Astron. Soc.* **473** (1), 198–209.

FORSLUND, D. W. & SHONK, C. R. 1970 Formation and structure of electrostatic collisionless shocks. *Phys. Rev. Lett.* **25**, 1699–1702.

GRASSI, A., GRECH, M., AMIRANOFF, F., PEGORARO, F., MACCHI, A. & RICONDA, C. 2017 Electron Weibel instability in relativistic counterstreaming plasmas with flow-aligned external magnetic fields. *Phys. Rev.* E **95** (2), doi:10.1103/PhysRevE.95.023203.

JACKSON, J. D. 1998 *Classical Electrodynamics*. Wiley.

KATO, T. N. 2007 Relativistic collisionless shocks in unmagnetized electron–positron plasmas. *Astrophys. J.* **668** (2), 974.

LEMOINE, M., GREMILLET, L., PELLETIER, G. & VANTHIEGHEM, A. 2019 Physics of Weibel-mediated relativistic collisionless shocks. *Phys. Rev. Lett.* **123**, 035101.

LICHTENBERG, A. J. & LIEBERMAN, M. A. 2013 *Regular and Chaotic Dynamics*. Springer.

LYUBARSKY, Y. & EICHLER, D. 2006 Are Gamma-ray bursts mediated by the Weibel instability? *Astrophys. J.* **647**, 1250.

MEDVEDEV, M. V. & LOEB, A. 1999 Generation of magnetic fields in the relativistic shock of gamma-ray burst sources. *Astrophys. J.* **526**, 697.

NOVO, A. S., BRET, A. & SINHA, U. 2016 Shock formation in magnetised electron–positron plasmas: mechanism and timing. *New J. Phys.* **18** (10), 105002.

OTT, E. 2002 *Chaos in Dynamical Systems*. Cambridge University Press.

RAM, A. K. & DASGUPTA, B. 2010 Dynamics of charged particles in spatially chaotic magnetic fields. *Phys. Plasmas* **17** (12), 122104.

RYUTOV, D. D. 2018 Collisional and collisionless shocks. *Plasma Phys. Control. Fusion* **61** (1), 014034.

SAGDEEV, R. Z. & KENNEL, C. F. 1991 Collisionless shock waves. *Sci. Am.* **264** (4), 40–47.

SHAISULTANOV, R., LYUBARSKY, Y. & EICHLER, D. 2012 Stream instabilities in relativistically hot plasma. *Astrophys. J.* **744**, 182.

SILVA, L. O., FONSECA, R. A., TONGE, J. W., DAWSON, J. M., MORI, W. B. & MEDVEDEV, M. V. 2003 Interpenetrating plasma shells: near-equipartition magnetic field generation and nonthermal particle acceleration. *Astrophys. J.* **596**, L121–L124.

SPITKOVSKY, A. 2008 Particle acceleration in relativistic collisionless shocks: Fermi process at last? *Astrophys. J. Lett.* **682**, L5–L8.

STOCKEM, A., LERCHE, I. & SCHLICKEISER, R. 2006 On the physical realization of two-dimensional turbulence fields in magnetized interplanetary plasmas. *Astrophys. J.* **651** (1), 584.

WIERSMA, J. & ACHTERBERG, A. 2004 Magnetic field generation in relativistic shocks. An early end of the exponential Weibel instability in electron–proton plasmas. *Astron. Astrophys.* **428**, 365–371.

YALINEWICH, A. & GEDALIN, M. 2010 Instabilities of relativistic counterstreaming proton beams in the presence of a thermal electron background. *Phys. Plasmas* **17**, 062101.

ZEL'DOVICH, I. A. B. & RAIZER, Y. P. 2002 *Physics of Shock Waves and High-Temperature Hydrodynamic Phenomena*. Dover Publications.

https://doi.org/10.1017/S0022377820000045 Published online by Cambridge University Press